Double electron capture in O^{6+} + He collisions

M. X. Ma,[1,2,*] T. Meng,[1,*] B. Tu,[1] P. Ma,[1] Y. W. Zhang,[3] L. Liu,[2,†] J. Xiao,[1] K. Yao,[1] Y. Zou,[1] Y. Wu,[2,3] J. G. Wang,[2] and B. Wei[1,‡]

[1]*Institute of Modern Physics, Key Laboratory of Nuclear Physics and Ion-Beam Application (MOE), Fudan University, Shanghai 200433, China*

[2]*Institute of Applied Physics and Computational Mathematics, P. O. Box 8009-26, Beijing 100088, China*

[3]*Center for Applied Physics and Technology, HEDPS, and School of Physics, Peking University, Beijing 100871, China*

(Received 11 January 2024; accepted 25 July 2024; published 10 September 2024)

As one kind of ubiquitous collision system, O^{6+} + He deserves attentive study due to its theoretical significance in fundamental physics and applied value in fields like astrophysics or plasma physics. Specifically, in the case of the electron capture process, while a considerable number of measurements and calculations have focused on single electron capture, research is still inadequate on the double electron capture which contributes nearly 10% to the overall electron capture. In this work, a two-active-electron semiclassical asymptotic-state close-coupling method is used to calculate the total and $l-$resolved state-selective double electron capture cross sections of O^{6+} + He collisions in the energy range 0.5–100 keV/u, accompanied by experimental measurements in the energy range 2.63–37.5 keV/u with an uncertainty of 16%, in good consistency. These theoretical and experimental data can fill gaps in the database of double electron capture in O^{6+} + He collisions and provide insights for improving theoretical models in further research.

DOI: 10.1103/PhysRevA.110.032806

I. INTRODUCTION

Collisions between highly charged ions (HCIs) and atoms/molecules have received great attention in recent decades due to advancements in HCI source technology. In particular, electron capture (EC), a dominant collision mechanism when the impact velocity is less than nearly one atomic unit [1], has been of considerable interest. To be more specific, as one of the main impurity ions in nuclear fusion devices, O^{6+} ions are frequently detected at present tokamak plasma edges and divertors [2–5]. These impurity ions may undergo EC processes with helium particles, which are abundant as products of *D-T* fusion reactions. Studies on their state-selective cross sections can be exploited for diagnosing impurity density through measured emission spectra [6] and assessing their influence on plasma operations. In addition, O^{6+} ions are of great abundance in the solar wind [7,8], as well as helium in the exospheres of astrophysical objects like Jupiter [9]. EC events between these kinds of particles in the solar wind and neutral gas materials are confirmed as important sources of extreme ultraviolet and soft x-ray emissions from astrophysical objects [10–12]. To better analyze the spectral lines in astrophysics, an accurate and comprehensive database of EC cross sections is also desirable.

At present, in contrast to the numerous calculations and experiments carried out on the single electron capture (SEC) of O^{6+} + He [13–19], scarce attention has been given to the double electron capture (DEC) process, which can be written as

$$O^{6+}(1s^2) + He(1s^2) \rightarrow O^{4+}(1s^2nln'l') + He^{2+}. \quad (1)$$

This lack of emphasis may come from the inherent low cross sections of DEC compared with SEC. However, based on our results, the cross sections of DEC can account for approximately 10% of the total EC process and should not be ignored in order to achieve a more precise spectrum analysis.

What is more, owing to weak reaction cross sections from DEC channels [20,21], it has been challenging to provide high-precision state-selective DEC results. For the vacuum ultraviolet photon-emission spectroscopy [17,18] or Auger spectroscopy [22] with a limited detective angle, long-time detection and low background are required if a relatively weak reaction process is studied, which brings many difficulties in carrying out the experiment technically. Moreover, Auger spectroscopy cannot provide information of DEC, a process that is followed by the process of radiative decay. To overcome these challenges, a methodology was established, allowing for the direct judgement of the state selectivity of captured electrons by the momentum measurement of recoil ions along the projectile direction with a 4π detective angle [23,24]. In present experiments, a cold target recoil ion momentum spectroscopy (COLTRIMS) is employed to reconstruct the momentum of recoil ions, achieving a good state-selective resolution. The total and state-selective cross sections of DEC in O^{6+} + He have been measured experimentally in the impact energy range of 2.63–37.5 keV/u.

With regard to theoretical perspective, only Machacek [20] has reported the total DEC cross sections using the $n-$electron classical trajectory Monte Carlo method (CTMC).

*These authors contributed equally.
†Contact author: liu_ling@iapcm.ac.cn
‡Contact author: brwei@fudan.edu.cn

This method simulates the collision between the projectile and the target within the framework of classical physics, ignoring the quantum effect, and the state-selective cross sections cannot be given accurately due to the fact that the determination of quantum number (n, l, m) of the captured electron is based on the quantum-classical correspondence principle. In this work, the measured results are compared with those calculated by a two-active-electron semiclassical asymptotic-state close-coupling (SCASCC) method. It has been successfully used to calculate SEC for O^{6+} + He [19]. SCASCC is a semiclassical nonperturbative method based on solving the eikonal equation. This equation can be solved by inserting the electronic wave function which is expanded by the asymptotic state, including reaction channels like excitation and electron transfer as much as possible. Comparing with the previous atomic close-coupling method based on a single active electron [13], the present electronic wave function is constructed by two active electrons. Therefore, it can describe the DEC process and provide cross sections for different DEC reaction channels. Furthermore, it is advantageous for assessing the accuracy of the theory regarding DEC process through comparison with experimental data.

The present article is organized as follows: The experimental setup is described in Sec. II. A brief introduction of the two-electron SCASCC method is given in Sec. III, and the basis sets and model potential are also reported. In Sec. IV, experimental and theoretical DEC cross sections are presented and compared with other available data. Conclusions are given at last. Atomic units will be used throughout this article, unless explicitly indicated.

II. EXPERIMENTAL METHOD

The experiments have been conducted at the Highly Charged Ions Collision Platform at Fudan University [21,25]. The platform comprises a 14.5-GHz electron cyclotron resonance (ECR) ion source capable of providing a HCI beam within an acceleration field ranging 5–150 kV. Two beam lines are utilized: beam line A, equipped with a gas cell for measuring total DEC cross sections, and beam line B, housing COLTRIMS for state-selective EC cross sections measurements. The background vacuum of beam lines is maintained at a level better than 10^{-6} Pa. Figure 1 describes the overall experimental setup.

In short, oxygen ions are extracted from the ECR at the desired energy. After mass charge selected by a 90° magnetic analyzer, a collimated beam of O^{6+} ions can enter either beam line A or B depending on whether a 45° magnetic analyzer is activated.

Detailed introduction for beam lines A and B can be found in our previous work [19]. In essence, beam line A is built based on the growth-rate method [26,27], which can measure the total DEC cross sections using the equation

$$F_{q-2} = \frac{\sigma_{q,q-2} l}{kT} P. \tag{2}$$

Here q is the initial charge state of projectiles. F_{q-2} stands for the fraction of scattered oxygen ions with charge of $q-2$ to the total. $\sigma_{q,q-2}$ is the total DEC cross sections. P and l are the pressure and length in the gas cell, respectively. k is the Boltzmann constant, and T is the temperature of target gas in units of kelvin. As l, k, and T are all known constants during the experiments, $\sigma_{q,q-2}$ can be derived from the linear relationship of F_{q-2} as a function of P. The total error of $\sigma_{6,4}$ is estimated to be about 16% which has been analyzed in detail elsewhere [21].

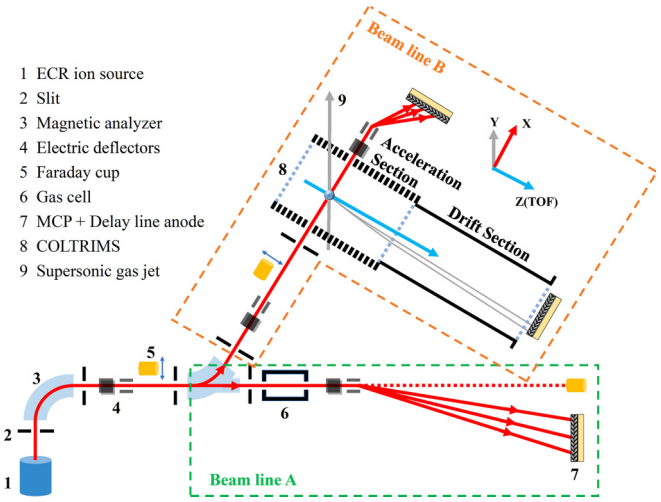

FIG. 1. Schematic drawing of the experimental apparatus.

As for beam line B equipped with COLTRIMS [28,29], different EC channels are identified through the coincidence measurements between each scattered oxygen ion and recoil helium ion with different charge states. The three-dimensional momenta of recoil He ions are then reconstructed. Due to the conservation of energy and momentum in one DEC collision, the momentum p_X along the projectile direction of each recoil He^{2+} ion is discrete and has a specific relation with the state selectivity of captured electrons, which follows

$$p_X = -\frac{Q_1 + Q_2}{v} - v, \tag{3}$$

where v is the velocity of projectiles, and Q_1 or Q_2 is the binding energy difference of each captured electron defined as $Q = \varepsilon_f - \varepsilon_i$ (ε_i and ε_f are the binding energy of the captured electron in the initial ground-state target and the final excited ion, respectively). Thus, the state selectivity in DEC can be directedly measured through the p_X distribution of He^{2+} given by COLTRIMS. Combined with the absolute total DEC cross sections, the state-selective ones can then be normalized. The uncertainties of state-selective DEC cross sections mainly result from the error in measuring $\sigma_{6,4}$ and the statistical error in counting recoil He^{2+} ions.

It is noteworthy that all measured DEC cross sections have not considered the autoionization double capture (ADC) channel. Due to the long distance between the collision zone and the following electric deflector exit (approximately 220 and 280 mm in beam lines A and B, respectively), the drift time of scattered ions before getting charge analyzed is larger than 0.8×10^{-7} s, which far exceeds 10^{-12}–10^{-15} s, the typical time scale of Auger decay process [30,31] after two electrons are captured into an autoionization state like $2pnl$ ($n \geqslant 6$) or $3lnl$ [22,32].

III. THEORETICAL METHOD

In this section, we introduce the two-active-electron semiclassical asymptotic-state close-coupling method [33–38] briefly.

Under the impact parameter approximation, the two electrons time-dependent Schrödinger equation can be reduced as

$$\left[H_e - i\frac{\partial}{\partial t}\right]\Psi(\vec{r_1}, \vec{r_2}, t) = 0 \tag{4}$$

with the electronic Hamiltonian H_e,

$$H_e = \sum_{i=1,2}\left[-\frac{1}{2}\nabla_i^2 + V_T(\vec{r}_i) + V_P\left(\vec{r}_i^{\,p}\right)\right] + \frac{1}{|\vec{r}_1 - \vec{r}_2|}. \tag{5}$$

$\vec{r}_i$ is the position vector of electron which is close to the target. $\vec{r}_i^{\,p} = \vec{r}_i - \vec{R}(t)$ is the position vector of the electron with respect to the projectile. The relative projectile-target position $\vec{R}(t)$ is defined as $\vec{R}(t) = \vec{b} + \vec{v}t$, where $\vec{b}$ and $\vec{v}$ are the impact parameter and velocity, respectively.

The interaction between electrons with target and projectile are represented by V_T and V_P, respectively. For this work, these potentials [39,40] are expressed as

$$V_{\mathrm{He}}(r) = -\frac{2}{r}, \tag{6}$$

$$V_{O^{6+}}(r) = -\frac{6}{r} - \frac{2}{r}(1 + 33.60r)e^{-16.80r}. \tag{7}$$

Equation (4) is solved by expanding the wave function accordingly on a set of electronic states of isolated collision partners,

$$\Psi(\vec{r_1}, \vec{r_2}, t) = \sum_{i=1}^{N^{TT}} c_i^{TT}(t)\Phi_i^{TT}(\vec{r_1}, \vec{r_2})e^{-iE_i^{TT}t} + \sum_{j=1}^{N^{PP}} c_j^{PP}(t)\Phi_j^{PP}(\vec{r_1}, \vec{r_2}, t)e^{-iE_j^{PP}t}$$
$$+ \sum_{k=1}^{N^T}\sum_{\mathrm{m}=1}^{N^P} c_{km}^{N^T N^P}(t)\left[\Phi_k^T(\vec{r_1})\Phi_{\mathrm{m}}^P(\vec{r_2}, t) + \Phi_k^T(\vec{r_2})\Phi_{\mathrm{m}}^P(\vec{r_1}, t)\right]e^{-i\left(E_k^T + E_m^P\right)t}, \ \# \tag{8}$$

where the superscripts T and TT (P and PP) denote that the states and corresponding energies for one or two electrons are on the target (projectile), respectively. For both electrons, the projectile states contain plane-wave electron translation factors $e^{i\vec{v}\cdot\vec{r}_i - i\frac{1}{2}v^2 t}$ in order to ensure Galilean invariance of the results. After inserting the wave function into Eq. (4), a first-order coupled differential equations can be obtained, written in matrix form as

$$i\frac{d}{dt}\mathbf{c}(t) = \mathbf{S}^{-1}(\vec{b}, \vec{v}, \mathrm{t})\mathbf{M}(\vec{b}, \vec{v}, \mathrm{t})\mathbf{c}(t). \tag{9}$$

After calculating the overlap and coupling matrix elements for a given b and v, the expansion coefficient c can be obtained by solving Eq. (9). Therefore, the expansion coefficient c is dependent on parameters b and v indirectly, where $\boldsymbol{c}$ is the column vector of the time-dependent expansion coefficients, and $\boldsymbol{S}$ and $\boldsymbol{M}$ are the overlap and coupling matrices, respectively.

Then the probability for a transition from the initial state i to a final state f is given by

$$P_{fi}(b, v) = \lim_{t\to\infty} |c_f(t)|^2. \tag{10}$$

The corresponding cross sections are then calculated from the above probabilities as

$$\sigma_{fi}(v) = 2\pi \int_0^{+\infty} bP_{fi}(b, v)db. \tag{11}$$

In the present calculations, the determination of electronic states centered on the target and projectile is performed using the variational method with Gaussian-type orbitals (GTOs). A set of 77 GTOs (12 for $l = 0$, 8×3 for $l = 1$, 4×5 for $l = 2$, and 3×7 for $l = 3$) is used on the projectile (O) center, and a set of 22 GTOs (10 for $l = 0$ and 4×3 for $l = 1$) is used on the target (He) center. These can allow the inclusion of 147 TT (two electrons on He), 1144 TP (one electron on He^+ and the other electron on O^{5+}), and 1583 PP (two electrons on O^{4+}) states in calculations. The eigenvalues of states on the O^{4+} ion are presented in Table I, and are compared with the corresponding experimental data from NIST tables [41] and Ref. [42]. It should be mentioned that the O^{4+} first ionization threshold [43] is −5.076 a.u. in our scale. The states which are lower than $2p5d$ are bound states from NIST. In the present work, considering the calculate error, the states classified as those below $2p5d$ are regarded as bound states even though their calculated energies are higher than −5.076 a.u.

The convergence of the GTOs is also checked by calculating the cross sections with different size GTO basis sets at the different collision energies. The present results have been compared with those from a larger basis set (82 GTOs (12 for $l = 0$, 8×3 for $l = 1$, 5×5 for $l = 2$, and 3×7 for $l = 3$) on the center of target and same basis on projectile). The total DEC cross sections from these two sets agree with each other within 3% and, for the dominant $l-$resolved state-selective double electron capture cross sections, disagreement is less than 25%.

IV. RESULTS AND DISCUSSION

A. Total DEC cross sections

The present experimental and theoretical total DEC cross sections are shown as a function of impact energy in Fig. 2. As far as we know, only the cross sections at 1.17 and 2.33 keV/u reported by Machacek *et al.* [20] and a few points reported by Crandall *et al.* [44] can be compared. The present

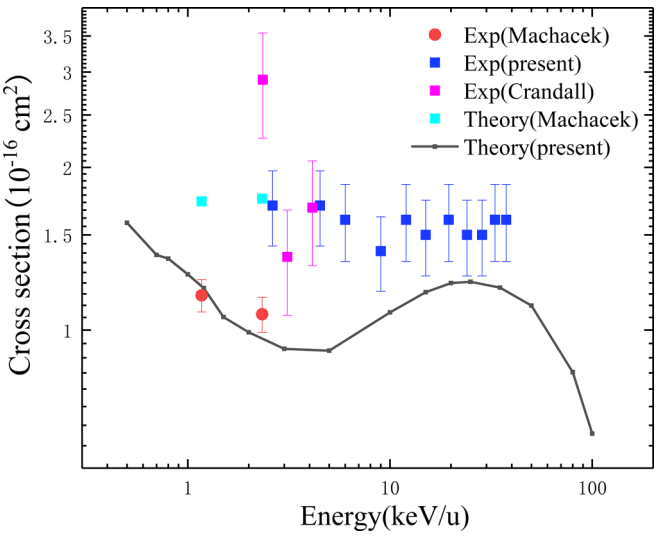

FIG. 2. Total DEC cross sections $\sigma_{6,4}$ of O^{6+} colliding with He as a function of the impact energy.

experimental results exhibit little variation in the energy range 2.63–37.5 keV/u and align with the theoretical calculations of Machacek at 2.33 keV/u. However, a significant difference exists, especially in 2–10 keV/u, where the present experimental value is maximally 78% larger than the present theoretical one. One possible reason for the discrepancy is the limitation of the used basis in present theoretical calculations. To be more specific, the calculated total cross sections do not include the contributions from $2s5g$ and $2snl$ ($n \geqslant 6$) states, except for $2s6s$ and $2s6p$ states. According to the data from NIST [41] and Ref. [42], these neglected states are probably bound states and have a non-negligible contribution. As Fig. 4 shows, the cross sections of $2s5l$ and above level can contribute nearly 50% to the entire DEC at 2.625 keV/u and decrease to 30% as the energy increases. This indicates that the neglected states in the basis may have a substantial influence on calculated outcomes in a comparatively low energy region. Moreover, the omission of successive electron capture processes in our calculation may also lead to the difference. Roncin *et al.* [45] pointed out in their study that correlated transfer-excitation (CTE) was a dominant process for this collision system under the incident energy of 0.56 keV/u. With the energy increases, the contribution from the correlated double capture (CDC) process becomes important [22,46]. The agreement between experimental and theoretical values in Fig. 4 further indicates that CDC is a dominant process for this collision system.

Additionally, when the two electrons of the He atom are captured into autoionization states of O^{4+} ions, they can deexcite through two different ways [45,47]. The $n-$symmetric states where the electrons occupy similar n shells tend to decay through Auger emission and produce O^{5+} ions, which is known by the autoionization double capture (ADC) process. Conversely, the $n-$asymmetric states have high probability to decay rapidly by photon emission. Then both electrons remain on the projectile (O^{4+} ions), which is known by the true double capture (TDC) process. The cross sections from the TDC process have not been included in the present calculations. However, the previous studies have pointed out that the stabilization ratio $R = \sigma\mathrm{TDC}/(\sigma\mathrm{TDC} + \sigma\mathrm{ADC})$ reaches 76% at 0.56 keV/u [45] and 68% at 6 keV/u [47], respectively. The high R value for this collision system is mainly due to

TABLE I. Comparison of energies (in a.u.) of O^{4+} states obtained in this work with the NIST [41] and bold data in italics are from Ref. [42]. Diff $= (E - E_{\mathrm{Ref}})/E$.

Config	Term	E_{Ref} [41,42]	E	Diff(%)	Config	Term	E_{Ref} [41,42]	E	Diff (%)
$1s^22s^2$	^1S	−9.2615	−9.2700	0.09%	$1s^22p4s$	^1P	−5.5058	−5.4808	−0.46%
$1s^22s2p$	^1P	−8.5379	−8.5041	−0.40%	$1s^22p4p$	^1S	−5.4368	−5.4611	0.45%
$1s^22p^2$	^1D	−8.2057	−8.1445	−0.75%	$1s^22p4p$	^1P	−5.4816	−5.4458	−0.66%
$1s^22p^2$	^1S	−7.9497	−7.8867	−0.80%	$1s^22p4p$	^1D	−5.4439	−5.4064	−0.69%
$1s^22s3s$	^1S	−6.7041	−6.7113	0.11%	$1s^22p4d$	^1P	−5.4002	−5.3983	−0.03%
$1s^22s3p$	^1P	−6.6151	−6.6127	−0.04%	$1s^22p4d$	^1D	−5.4440	−5.3978	−0.86%
$1s^22s3d$	^1D	−6.4702	−6.4648	−0.08%	$1s^22p4f$	^1F		−5.3920	
$1s^22p3s$	^1P	−6.2339	−6.2064	−0.44%	$1s^22p4f$	^1G	−5.4071	−5.3824	−0.46%
$1s^22p3p$	^1P	−6.1965	−6.1609	−0.58%	$1s^22p4f$	^1D		−5.3756	
$1s^22p3d$	^1D	−6.0965	−6.0594	−0.61%	$1s^22p4d$	^1F	−5.4016	−5.3543	−0.88%
$1s^22p3p$	^1D	−6.0849	−6.0470	−0.63%	$1s^22s6s$	^1S	***−5.4391***	−5.3474	−1.71%
$1s^22p3p$	^1S	−6.0373	−6.0151	−0.37%	$1s^22s6p$	^1P	−5.4359	−5.3437	−1.72%
$1s^22p3d$	^1F	−6.0130	−5.9770	−0.60%	$1s^22p5s$	^1P	***−5.1700***	−5.1906	0.40%
$1s^22p3d$	^1P	−5.9842	−5.9474	−0.62%	$1s^22p5p$	^1P	−5.1673	−5.1480	−0.37%
$1s^22s4s$	^1S	−5.9277	−5.9187	−0.15%	$1s^22p5p$	^1D	−5.1497	−5.1003	−0.97%
$1s^22s4p$	^1P	−5.8995	−5.8941	−0.09%	$1s^22p5d$	^1D	−5.1485	−5.0875	−1.20%
$1s^22s4d$	^1D	−5.8612	−5.8469	−0.24%	$1s^22p5p$	^1S	***−5.1255***	−5.0837	−0.82%
$1s^22s4f$	^1F	−5.8450	−5.8425	−0.04%	$1s^22p5f$	^1F	***−5.1305***	−5.0801	−0.99%
$1s^22s5s$	^1S	***−5.6127***	−5.6312	0.33%	$1s^22p5f$	^1G	***−5.1244***	−5.0722	−1.03%
$1s^22s5p$	^1P	−5.6052	−5.5948	−0.19%	$1s^22p5f$	^1D	***−5.1232***	−5.0665	−1.12%
$1s^22s5f$	^1F	−5.5758	−5.5493	−0.48%	$1s^22p5d$	^1F	−5.1316	−5.0470	−1.68%
$1s^22s5d$	^1D	−5.5784	−5.5361	−0.76%	$1s^22p5d$	^1P	***−5.1181***	−5.0321	−1.71%

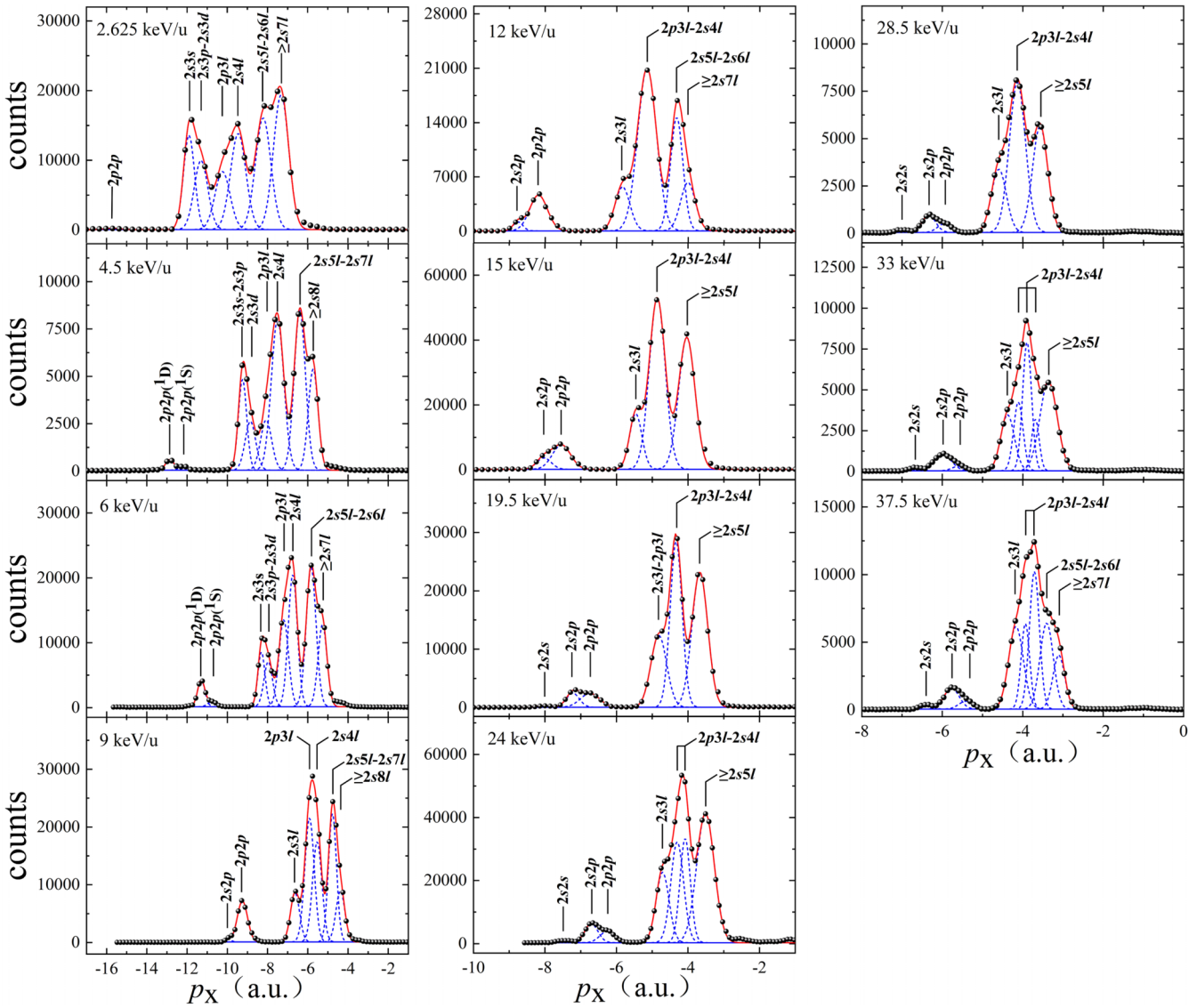

FIG. 3. Measured X-dimension momentum spectra of recoil He^{2+} ions at different collision energies. Solid black dots are experimental data and red lines are final results of multipeak Gaussian fitting. To distinguish overlapping peaks, blue dashed lines are used standing for the single Gaussian peaks of different final electron states.

TABLE II. Measured total and state-selective DEC cross sections for O^{6+} colliding with He. (Note: All cross sections are in units of 10^{-16} cm^2, and energies in keV/u. Autoionization states are not included.)

		$\sigma_{6,4}(nln'l')$						
Energy	$\sigma_{6,4}$	$2s2s$	$2s2p$	$2p2p$	$2s3s$	$2s3l$	$2p3l$–$2s4l$	$\geqslant 2s5l$
2.625	1.7 ± 0.27			0.004 ± 0.003	0.218 ± 0.035	0.415 ± 0.066	0.491 ± 0.090	0.789 ± 0.126
4.50	1.7 ± 0.27			0.032 ± 0.008		0.326 ± 0.052	0.628 ± 0.101	0.715 ± 0.115
6.00	1.6 ± 0.26			0.075 ± 0.018	0.119 ± 0.019	0.239 ± 0.038	0.631 ± 0.101	0.656 ± 0.109
9.00	1.4 ± 0.22		0.006 ± 0.002	0.131 ± 0.021		0.140 ± 0.022	0.658 ± 0.105	0.465 ± 0.096
12.0	1.6 ± 0.26		0.021 ± 0.004	0.155 ± 0.025		0.160 ± 0.026	0.746 ± 0.119	0.518 ± 0.083
15.0	1.5 ± 0.24		0.040 ± 0.012	0.108 ± 0.019		0.167 ± 0.027	0.661 ± 0.106	0.525 ± 0.085
19.5	1.6 ± 0.26	0.006 ± 0.003	0.051 ± 0.015	0.075 ± 0.017		0.868 ± 0.139	0.599 ± 0.097	
24.0	1.5 ± 0.24	0.008 ± 0.004	0.062 ± 0.019	0.042 ± 0.017		0.229 ± 0.052	0.589 ± 0.139	0.570 ± 0.097
28.5	1.5 ± 0.24	0.010 ± 0.004	0.065 ± 0.017	0.035 ± 0.014		0.264 ± 0.042	0.676 ± 0.110	0.450 ± 0.077
33.0	1.6 ± 0.26	0.013 ± 0.003	0.074 ± 0.012	0.041 ± 0.007		0.251 ± 0.040	0.713 ± 0.114	0.507 ± 0.081
37.5	1.6 ± 0.26	0.018 ± 0.004	0.066 ± 0.011	0.057 ± 0.010		0.249 ± 0.040	0.781 ± 0.125	0.429 ± 0.069

TABLE III. Calculated total and state-selective DEC cross sections for O^{6+} colliding with He. (Note: All cross sections are in units of 10^{-16} cm^2, and energies in keV/u. Autoionization states are not included.)

		$\sigma_{6,4}(nln'l')$									
Energy	$\sigma_{6,4}$	$2s2s$	$2s2p$	$2p2p$	$2s3l$	$2s4l$	$2s5l$	$2p3l$	$2p4l$	$2p5l$	$2s6l$ ($l = s, p$)
0.5	1.5796	0.0001	0.0004	0.0031	0.0777	0.0711	0.1704	0.0953	0.5983	0.4818	0.0814
0.7	1.3776	0.0002	0.0006	0.0021	0.1044	0.1033	0.1302	0.1153	0.4761	0.4050	0.0405
0.8	1.3558	0.0002	0.0009	0.0020	0.1292	0.1061	0.1330	0.1242	0.4089	0.4065	0.0448
1	1.2680	0.0009	0.0007	0.0014	0.1658	0.0964	0.1247	0.1508	0.3500	0.3452	0.0320
1.2	1.1958	0.0004	0.0017	0.0023	0.2015	0.1030	0.1113	0.1467	0.3250	0.2752	0.0288
1.5	1.0571	0.0001	0.0004	0.0016	0.2033	0.1172	0.0992	0.1462	0.2643	0.2026	0.0221
2	0.9906	0.0001	0.0003	0.0026	0.2000	0.1229	0.0700	0.1711	0.2457	0.1605	0.0173
3	0.9233	0.0001	0.0007	0.0061	0.2082	0.1488	0.0945	0.1849	0.1599	0.1039	0.0163
5	0.9161	0.0003	0.0022	0.0231	0.1635	0.1712	0.0669	0.2335	0.1620	0.0733	0.0202
10	1.0788	0.0004	0.0134	0.0989	0.1444	0.1362	0.0262	0.3589	0.1957	0.0502	0.0544
15	1.1754	0.0010	0.0316	0.0798	0.1627	0.1086	0.0202	0.4069	0.2509	0.0432	0.0707
20	1.2216	0.0041	0.0410	0.0476	0.2064	0.1090	0.0187	0.4011	0.2735	0.0493	0.0709
25	1.2289	0.0073	0.0391	0.0329	0.2240	0.1206	0.0193	0.4167	0.2729	0.0433	0.0528
35	1.1982	0.0098	0.0346	0.0325	0.2240	0.0978	0.0277	0.4479	0.2353	0.0643	0.0242
50	1.1100	0.0114	0.0377	0.0460	0.1972	0.0846	0.0291	0.4614	0.1659	0.0658	0.0108
80	0.8359	0.0092	0.0331	0.0718	0.1173	0.0742	0.0251	0.3174	0.1236	0.0567	0.0075
100	0.6436	0.0058	0.0246	0.0770	0.0749	0.0574	0.0244	0.2151	0.1045	0.0541	0.0058

the significant population of $2lnl$ ($n \geqslant 6$) configurations. As the incident energy increases, the population of $3l3l'$ states may become significant and can be comparable to those of $2lnl$ ($n \geqslant 6$) configurations. Thus, the smaller contribution from the deexcitation of these states through photon emission causes the convergence between theoretical results and the experimental data. It can also be one of the reasons for the disagreement between the theoretical SEC cross sections and the experimental ones in the high-energy region [19]. Thus, the reasons mentioned above along with the experimental error of 16% lead to the noticeable difference between the present experimental and theoretical results. Further investigations are still needed to confirm this.

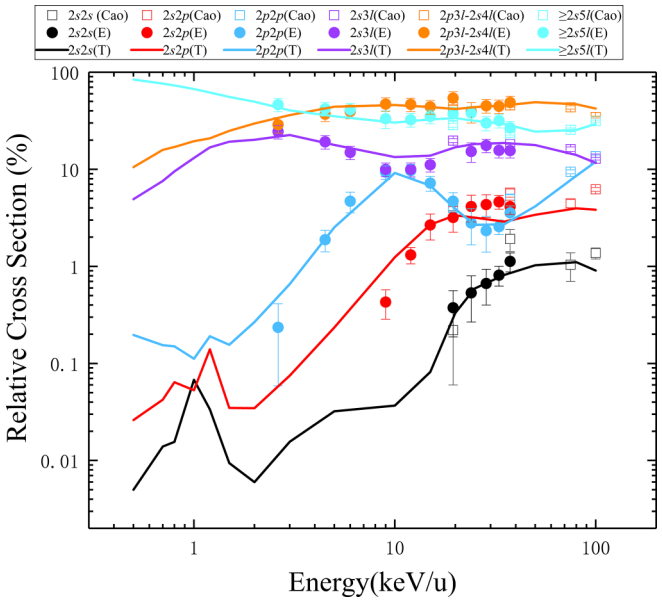

FIG. 4. The comparable relative state-selective DEC cross sections as a function of the impact energy.

B. *n*- and *nl*-state-selective DEC cross sections

The total DEC cross sections give the probability that two electrons are captured during the collision process, but without the information about their final states (nl, $n'l'$). Based on COLTRIMS, the distribution of final states of the two transferred electrons is measured through the recoil momentum of He^{2+} and presented in Fig. 3. In order to distinguish overlapped states as fine as possible, multipeak Gaussian fitting is applied when dealing with the recoil momentum spectrum. In general, the position and width of every single Gaussian peak are fixed when fitting an area with dense peaks. The accurate value of the position of each state can be calculated through Eq. (3), and the width of a well-separated single state like $2p2p$ can be a proper reference for other states. As for one peak containing multiple states, its position is slightly optimized from the average value of calculated positions, and its width is expanded based on their position difference to reach a better fitting of R^2.

In the energy range 2.63–37.5 keV/u, these electrons from the neutral He are primarily captured into $2s3l$ and higher energy levels (autoionization states are not considered). With the increase of collision energy, the channels of both electrons being captured into the $n = 2$ subshell gradually open up and contribute more to the overall DEC process. For the convenience of application, all measured and calculated data, including the total and state-selective DEC cross sections, are listed in Tables II and III, respectively.

Since we have no correlated absolute DEC state-selective data for comparison, Fig. 4 presents the relative cross sections of state-selective DEC together with those measured using the same method by Cao *et al.* [48]. General agreement is achieved between the present results and the experimental

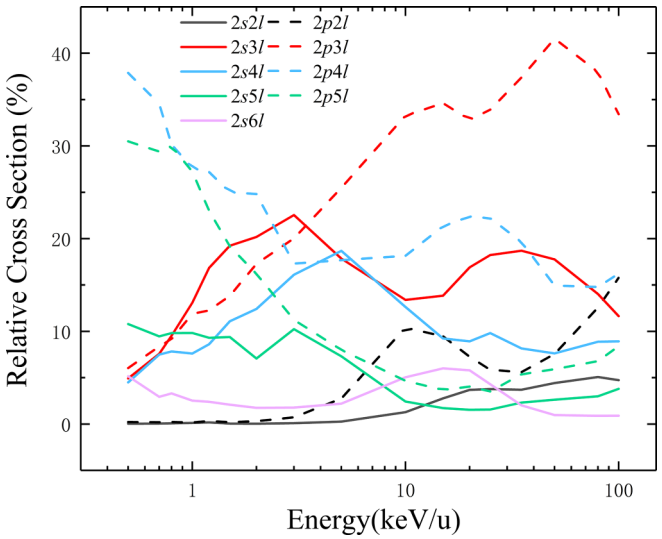

FIG. 5. The calculated relative state-selective DEC cross sections as a function of the impact energy. As mentioned before, 5*g* and 6*l* (except for *s* and *p*) are not included.

ones from [48] at 19.5, 37.5, 75, and 100 keV/u. In the present results, cross sections of the $2s2s$ and $2s2p$ channels grow dramatically with the increase of energy and flatten out at nearly 20 keV/u. There are three peaks for $2lnl$ states around 1 keV/u, however, the accuracy of the present calculation may not be enough given the minor contribution to the relative cross section; the use of logarithmic scale exaggerates the difference, particularly at the adjacent two points where they do not align. Consequently, the reliability of these peaks may be questionable. For $2s3l$ and higher energy states, their contributions comparatively remain steady. Rich trends are observed in the $2p2p$ channel, where its cross sections reach a maximum at 10 keV/u and rebound at 30 keV/u. The measured tendencies of different channels align well with the calculated ones.

A more detailed description of the state-selective DEC cross section can be found in Fig. 5. This figure only shows the theoretical results since the experimental challenge lies in distinguishing the single l-state momentum peak when energy levels get higher and denser. Under the independent electron approximation (IEA), the electrons are captured independently and expected in the same or neighboring shells, however, the existence of electronic correlations cause the IEA's predictions to deviate from the actual situation, leading to asymmetric states. In other words, electronic correlations were involved in the formation of the configurations, especially for asymmetric states. The considered channels can be divided into two main groups: one group stands for the electron of lower energy always staying in the $2s$ state (solid lines), while another group stands for the lower one which always stays in the $2p$ state (dashed lines). Generally, the cross sections from $2pnl$ states are larger than those of $2snl$ states for the same n quantum number. This could be attributed to their similar energies, but the former have more available coupling states. Below 3 keV/u, the dominant channels are $2p4l$ and $2p5l$, while the $2s3l$ state reaches its maximum. With increasing impact energy, the $2p3l$ channel becomes increasingly significant and far surpasses the second candidate.

V. CONCLUSION

In the present work, the investigation of the DEC process in collisions of O^{6+} with He is performed both experimentally and theoretically. The total cross sections for two electrons captured into O^{4+} ($1s^2nln'l'$) from neutral He have been measured with an uncertainty of 16% in the energy range 2.63–37.5 keV/u. Additionally, the branch ratios of different DEC state-selective channels have been obtained from the He^{2+} recoil momentum distribution measured by COLTRIMS. Total and state-selective cross sections are also calculated by a two-active-electron semiclassical asymptotic-state close-coupling method in the energy range 0.3–100 keV/u. General agreement between the present experimental and theoretical results is obtained for the relative state-selective ones in the overlapping energy range, while an obvious discrepancy exists in the total DEC cross sections. Electrons tend to be captured into $2pnl$ states rather than $2snl$, in particular, the $2p3l$ state is the most significant channel above 3 keV/u. These energy-dependent total and state-selective DEC cross sections can provide essential data for the analysis of spectral emission and plasma simulations in the current tokamaks, astronomical objects, etc.

ACKNOWLEDGMENTS

This work was supported by the National Key R&D Program of China under Grant No. 2022YFA1602504, the National Natural Science Foundation of China (Grants No. 12274040 and No. U1832201), and Shanghai Leading Academic Discipline Project (Project No. B107).

[1] J. B. Greenwood, R. J. Mawhorter, I. Čadež, J. Lozano, S. J. Smith, and A. Chutjian, The contribution of charge exchange to extreme ultra-violet and x-ray astronomy, Phys. Scr. T **110**, 358 (2004).

[2] M. E. Puiatti, C. Breton, C. De Michelis, and M. Mattioli, Impurity charge-exchange processes in Tokamak plasmas, Plasma Phys. **23**, 1075 (1981).

[3] G. F. Matthews, Impurity production and transport at limiters, J. Nucl. Mater. **162–164**, 38 (1989).

[4] M. K. Pandey, Y.-C. Lin, and Y. K. Ho, Investigation of charge transfer and ionization in He-like systems (Li^+, Be^{2+}, B^{3+}, C^{4+}, N^{5+}, O^{6+})-hydrogen atom collisions in Debye plasmas, Phys. Plasma. **20**, 022104 (2013).

[5] A. Bhattacharya, J. Ghosh, M. B. Chowdhuri, and P. Munshi, Numerical estimation of the oxygen impurity transport in the Aditya tokamak, Phys. Plasmas. **27**, 023303 (2020).

[6] J. D. Hey, C. C. Chu, S. Brezinsek, P. Mertens, and B. Unterberg, Oxygen ion impurity in the TEXTOR tokamak

boundary plasma observed and analysed by Zeeman spectroscopy, J. Phys. B: At. Mol. Opt. Phys. **35**, 1525 (2002).

[7] R. Von Steiger, N. A. Schwadron, L. A. Fisk, J. Geiss, G. Gloeckler, S. Hefti, B. Wilken, R. R. Wimmer-Schweingruber, and T. H. Zurbuchen, Composition of quasi-stationary solar wind flows from ulysses/solar wind ion composition spectrometer, J. Geophys. Res. Space Phys. **105**, 27217 (2000).

[8] G. Gloeckler and J. Geiss, The composition of the solar wind in polar coronal holes, Space Sci. Rev. **130**, 139 (2007).

[9] A. Moradmand, M. O. A. E. Ghazaly, D. P. Mahaptra, and A. Chutjian, Measurement of absolute single and double charge exchange cross sections for $Si^{(7-10)+}$ at 0.88–2.50 KeV/u impacting He and H_2, Astrophys. J. Suppl. Ser. **234**, 14 (2018).

[10] K. Dennerl, C. M. Lisse, A. Bhardwaj, V. Burwitz, J. Englhauser, H. Gunell, M. Holmström, F. Jansen, V. Kharchenko, and P. M. Rodríguez-Pascual, First observation of mars with XMM-Newton, Astron. Astrophys. **451**, 709 (2006).

[11] D. Koutroumpa, R. Lallement, J. C. Raymond, and V. Kharchenko, The solar wind charge-transfer x-ray emission in the 1/4 keV energy range: Inferences on local bubble hot gas at Low Z, Astrophys. J. **696**, 1517 (2008).

[12] G. Y. Liang, X. L. Zhu, H. G. Wei, D. W. Yuan, J. Y. Zhong, Y. Wu, R. Hutton, W. Cui, X. W. Ma, and G. Zhao, Charge-exchange soft X-ray emission of highly charged ions with inclusion of multiple-electron capture, Mon. Not. R. Astron. Soc. **508**, 2194 (2021).

[13] W. Fritsch and C. D. Lin, Atomic-orbital expansion study for the (quasi-)two-electron collision system O^{6+} + He and C^{6+} + He, J. Phys. B: At. Mol. Phys. **19**, 2683 (1986).

[14] N. Shimakura, H. Sato, M. Kimura, and T. Watanabe, Electron capture processes in collisions of O^{6+} with He using the travelling molecular orbital method, J. Phys. B: At. Mol. Phys. **20**, 1801 (1987).

[15] Y. Q. Zhao, L. Liu, P. Xue, J. G. Wang, and R. K. Janev, Polarization degrees of $3p^2\,P_{3/2}-3s^2\,S_{1/2}$ transition in $O^{5+}(1s^2\,3p)$ produced in collisions of O^{6+} with He and H_2, J. Phys. B: At. Mol. Opt. Phys. **43**, 185202 (2010).

[16] T. Iwai, Y. Kaneko, M. Kimura, N. Kobayashi, S. Ohtani, K. Okuno, S. Takagi, H. Tawara, and S. Tsurubuchi, Cross sections for one-electron capture by highly stripped ions of B, C, N, O, F, Ne, and S from He below 1 KeV/Amu, Phys. Rev. A **26**, 105 (1982).

[17] D. Dijkkamp, Y. S. Gordeev, A. Brazuk, A. G. Drentje, and F. J. de Heer, Selective single-electron capture into (n,l) subshells in slow collisions of C^{6+}, N^{6+}, O^{6+} and Ne^{6+} with He, H_2 and Ar, J. Phys. B: At. Mol. Phys. **18**, 737 (1985).

[18] J. P. M. Beijers, R. Hoekstra, and R. Morgenstern, State-selective charge transfer between He-like Ions and He, Phys. Rev. A **49**, 363 (1994).

[19] T. Meng, M. X. Ma, B. Tu, P. Ma, Y. W. Zhang, L. Liu, J. Xiao, K. Yao, Y. Zou, and Y. Wu, Study of single electron capture in O^{6+} + He collisions, New J. Phys. **25**, 093026 (2023).

[20] J. R. Machacek, D. P. Mahapatra, D. R. Schultz, Yu. Ralchenko, A. Chutjian, J. Simcic, and R. J. Mawhorter, Measurement and calculation of absolute single- and double-charge-exchange cross sections for O^{6+} ions at 1.17 and 2.33 keV/u impacting He and H_2, Phys. Rev. A **90**, 052708 (2014).

[21] J. Han, L. Wei, B. Wang, B. Ren, W. Yu, Y. Zhang, Y. Zou, L. Chen, J. Xiao, and B. Wei, Measurement of absolute single and double electron capture cross sections for O^{6+} Ion collisions with CO_2, CH_4, H_2, and N_2, Astrophys. J. Suppl. Ser. **253**, 6 (2021).

[22] N. Stolterfoht, C. C. Havener, R. A. Phaneuf, J. K. Swenson, S. M. Shafroth, and F. W. Meyer, Evidence for correlated double-electron capture in low-energy collisions of O^{6+} with He, Phys. Rev. Lett. **57**, 74 (1986).

[23] C. L. Cocke and R. E. Olson, Recoil ions, Phys. Rep. **205**, 153 (1991).

[24] V. Mergel, R. Dörner, J. Ullrich, O. Jagutzki, S. Lencinas, S. Nüttgens, L. Spielberger, M. Unverzagt, C. L. Cocke, R. E. Olson, M. Schulz, U. Buck, E. Zanger, W. Theisinger, M. Isser, S. Geis, and H. Schmidt-Böcking, State selective scattering angle dependent capture cross sections measured by cold target recoil ion momentum spectroscopy, Phys. Rev. Lett. **74**, 2200 (1995).

[25] Z. H. Xia, B. Ren, R. T. Zhang, L. Wei, J. Han, T. Meng, J. Wang, P. Ma, Y. Zhang, B. Tu, J. Xiao, K. Yao, Y. Zou, X. L. Zhu, D. L. Guo, X. Ma, and B. Wei, Measurement of $n-$ and $l-$resolved state-selective charge exchange in Ar^{8+} collision with He, Astrophys. J. **933**, 207 (2022).

[26] H. Tawara and A. Russek, Charge changing processes in hydrogen beams, Rev. Mod. Phys. **45**, 178 (1973).

[27] P.-F. Ma, J.-R. Wang, Z.-X. Zhang, T.-M. Meng, Z.-H. Xia, B.-H. Ren, L. Wei, K. Yao, J. Xiao, Y.-M. Zou, B.-S. Tu, and B.-R. Wei, Measurements of absolute electron capture cross sections in He^{2+}-He and Ne^{8+}–O_2, N_2, CH_4 collisions, Nucl. Sci. Technol. **34**, 156 (2023).

[28] R. Dörner, V. Mergel, O. Jagutzki, L. Spielberger, J. Ullrich, R. Moshammer, and H. Schmidt-Böcking, Cold target recoil ion momentum spectroscopy: A 'momentum microscope' to view atomic collision dynamics, Phys. Rep. **330**, 95 (2000).

[29] Y. Zhang, T. Jiang, L. Wei, D. Luo, X. Wang, W. Yu, R. Hutton, Y. Zou, and B. Wei, Three-body fragmentation of methane dications produced by slow Ar^{8+}-ion impact, Phys. Rev. A **97**, 022703 (2018).

[30] N. Vaeck and J. E. Hansen, Calculations for $1s^2 3l3l'$ states in C^{2+}, N^{3+}, O^{4+}, Ne^{6+} and Xe^{50+}, J. Phys. B: At. Mol. Opt. Phys. **22**, 3137 (1989).

[31] N. Nakamura, T. Nabeshima, F. J. Currell, Y. Kanai, S. Kitazawa, M. Koide, H. A. Sakaue, H. Ida, Y. Matsui, K. Wakiya, T. Takayanagi, T. Kambara, Y. Awaya, H. Suzuki, S. Ohtani, and U. I. Safronova, Ejected-electron spectra from the triplet states of O^{4+} ($1s^2 3l3l'$) produced by O^{6+} + O_2 collisions, J. Phys. B: At. Mol. Opt. Phys. **27**, L785 (1994).

[32] J.-Y. Chesnel, F. Frémont, B. Sulik, C. Ruiz-Méndez, H. Merabet, C. Bedouet, X. Husson, M. Grether, and N. Stolterfoht, Double-electron capture and radiative stabilization processes in slow ion–atom collisions, Nucl. Instrum. Methods Phys. Res. B **154**, 142 (1999).

[33] N. Sisourat, I. Pilskog, and A. Dubois, Nonperturbative treatment of multielectron processes in ion-molecule scattering: Application to He^{2+}-H_2 collisions, Phys. Rev. A **84**, 052722 (2011).

[34] J. W. Gao, Y. Wu, N. Sisourat, J. G. Wang, and A. Dubois, Single-and double-electron transfer in low-and intermediate-energy C^{4+} + He collisions, Phys. Rev. A **96**, 052703 (2017).

[35] J. W. Gao, Y. Wu, J. G. Wang, A. Dubois, and N. Sisourat, Double electron capture in H^+ + H^- collisions, Phys. Rev. Lett. **122**, 093402 (2019).

[36] J. W. Gao, Y. Y. Qi, Z. H. Yang Z. M. Hu, Y. W. Zhang, Y. Wu, J. G. Wang, A. Dubois, and N. Sisourat, Single-and double-electron capture in intermediate-energy $H^+ + Mg$ collisions, Phys. Rev. A **104**, 032826 (2021).

[37] Y. W. Zhang, J. W. Gao, Y. Wu, J. G. Wang, N. Sisourat, and A. Dubois, Single-and double-electron capture in intermediate-energy Ar^{8+} + He collisions, Phys. Rev. A **106**, 042809 (2022).

[38] J. W. Gao, Y. Y. Qi, Y. Wu, and J. G. Wang, Single-and double-electron capture cross sections for O^{6+} Ion in collisions with H_2 molecules, Astrophys. J. **944**, 167 (2023).

[39] G. Peach, H. E. Saraph, and M. J. Seaton, Atomic data for opacity calculations. IX. The lithium isoelectronic sequence, J. Phys. B: At. Mol. Opt. Phys. **21**, 3669 (1988).

[40] L. Liu, J. G. Wang, and R. K. Janev, State-selective electron capture in N^{5+}-H and O^{6+}-H collisions, J. Phys. B: At. Mol. Opt. Phys. **45**, 015202 (2011).

[41] A. Kramida, Yu Ralchenko, and J. Reader, and NIST ASD Team (2023); NIST Atomic Spectra Database (ver. 5.11), https://doi.org/10.18434/T4W30F.

[42] R. C. Mancini and U. I. Safronova, Rydberg series in Be-like ions ($1s^2$ 2lnl′, n = 5 − 12), J. Phys. B: At. Mol. Opt. Phys. **28**, 3469 (1995).

[43] H. Bachau, P. Galan, F. Martín, A. Riera, and M. Yáñez, Resonance parameters and properties of beryllium-like doubly excited states: $4 \leqslant Z \leqslant 10$, At. Data Nucl. Data Tables **44**, 305 (1990).

[44] D. H. Crandall, Electron transfer between He-like ions and He, Phys. Rev. A **16**, 958 (1977).

[45] P. Roncin, M. Barat, M. N. Gaboriaud, L. Guillemot, and H. Laurent, Collision spectroscopy of O^{6+} and N^{6+} colliding on a He target, J. Phys. B: At. Mol. Opt. Phys. **22**, 509 (1989).

[46] F. W. Meyer, C. C. Havener, R. A. Phaneuf, J. K. Swenson, S. M. Shafroth, and N. Stolterfoht, Evidence for correlated double-electron capture in slow collisions of multicharged ions with He and H_2, Nucl. Instrum. Methods Phys. Res. B **24**, 106 (1987).

[47] X. Ying-Li, Y. De-Yang, L. Rong-Chun, S. Cao-Jie, R. Fang-Fang, Y. Zhi-Hu, and C. Xiao-Hong, Two electron transfer and stabilization in slow O^{6+} and rare-gas collisions, Chin. Phys. Lett. **27**, 073402 (2010).

[48] T. Cao, T. Meng, Y. Gao, S. F. Zhang, R. T. Zhang, S. Yan, X. L. Zhu, J. Wang, P. Ma, B. Ren, Z. H. Xia, D. L. Guo, C. J. Zhang, K. Z. Lin, S. Xu, B. Wei, and X. Ma, State-selective charge exchange in 19.5–100 keV amu^{-1} O^{6+} collision with He and H_2, Astrophys. J. Suppl. Ser. **266**, 20 (2023).